Printed Stretchable Interconnects for Smart Garments: Design, Fabrication, and Characterization

Murat A. Yokus, Rachel Foote, and Jesse S. Jur

***Abstract*— This paper explores stretchability and fatigue life of inexpensive printed stretchable interconnects for smart garments. Multilayer stretchable interconnects are created on a knit fabric by screen printing of Ag/AgCl conductive inks on thermoplastic polyurethane film (TPU). Heat lamination of this layer onto a knit fabric and its protective encapsulation with a second TPU layer yields a multilayer stretchable interconnect structure. Design and optimization of the printed meandering interconnects are performed experimentally. The effect of processing steps, area of substrate, and encapsulation layers on the electro-mechanical properties of the stretchable interconnects are investigated. Washing endurance of the printed lines is also explored. The meandering stretchable printed line demonstrates stretchability of over 100% strain and fatigue life of 1000 cycles at 20% strain. Washing endurance of 100 cycles is reported. This paper presents an inexpensive method of realization of electronics integration on textiles by maintaining textile comfort and wearability.**

***Index Terms*— Flexible electronics, screen-printing, smart textiles, stretchable interconnects, wearable electronics.**

I. Introduction

WEARABLE electronics have been the focus of attention for researchers in the last couple decades. There is a significant growing interest in this field ranging from unobtrusive textile integrated bio-sensors [1], to electrochromic displays embedded into textiles [2]. Current research focuses on the use of nanotechnology, organic materials, and innovative fabrication techniques to create flexible electronic devices such as sensors [3], supercapacitors [4], conductive yarns [5], and energy harvesting devices [6]. These flexible devices are designed to bend and flex to form on curvilinear surfaces, which make them suitable for integration into textiles. The unobtrusive integration of discrete flexible devices into textiles creates a new norm for wearable technology, i.e., a smart garment.

There are key requirements that need to be fulfilled when creating a wearable smart garment. Air and vapor permeability, biocompatibility, comfort, washing and chemical (i.e., detergent) resistance, and ease of deformation (bending, compression, extension etc.) are indispensable necessities. Electro-mechanical durability of the smart garment when subjected to large strains is equally critical in determining the endurance of the garment to the dynamic forces of body movement. Prior research has shown that fabrics may experience up to ~20% strain during a set of various physical activities [7], [8]. Electronics positioned various locations of the fabric will undergo this range of deformation from the body's movement. Ideally, this deformation needs to happen through stretchable interconnects between the less resilient, hard electronic components. Therefore, the design of stretchable interconnects is important for maximizing the functionality while at the same time accommodating larger strains without constraining body movement for human comfort.

In order to provide stretchability without diminishing the functionality of electronic devices, various fabrication methods and stretchable material structures have been studied. Fabrication of wavy or buckled single crystal semiconductor nanoribbons [9] or metals [10] (e.g., gold) by pre-straining the elastomeric substrate, and mesh-shaped structures [11] yielded electronic device (e.g., thin film transistors and transistor-based pressure sensors) functionalities up to 25% strain values by undergoing out-of-plane deformation. These techniques have yielded hemispherical electronic eye cameras based on an array of silicon photodetectors [12]. However, the methods require complex component transferring and mechanical pre-straining the polymeric substrate. A different approach to make stretchable interconnects is to fabricate planar horseshoe shaped structures by lithographically patterning gold on elastomeric substrates [13]. Failure strain of 54% and cyclic endurance of 200 cycles at 25% strain have been achieved. Moreover, a photoablation method [14] was utilized to fabricate rectilinear and meandering interconnect designs. Its fabrication process used metal layers for polymer masking; therefore, eliminating the alignment process and use of chemicals for etching. However, the presence of conical defects was stated to have an effect on the stretchability of the meandering lines. A failure strain of 50% with a resistance change ($\Delta R/R$) of 5% was shown. As an alternative method for stretchable interconnects, liquid alloy filled elastomeric micro-channels

Manuscript received March 19, 2016; revised May 22, 2016 and June 7, 2016; accepted August 21, 2016. Date of publication September 14, 2016; date of current version October 13, 2016. This work was supported by the U.S. National Science Foundation through Nanosystems Engineering Research Center for Advanced Self-Powered Systems of Integrated Sensors and Technologies under Grant EEC 1160483. The associate editor coordinating the review of this paper and approving it for publication was Prof. Paul P. Sotiriadis. *(Corresponding author: Jesse S. Jur.)*

M. A. Yokus is with the Department of Electrical and Computer Engineering and the Department of Textile Engineering, Chemistry and Science, North Carolina State University, Raleigh, NC 27695 USA.

R. Foote and J. S. Jur are with the Department of Textile Engineering, Chemistry and Science, North Carolina State University, Raleigh, NC 27695 USA (e-mail: jsjur@ncsu.edu).

This paper has supplementary downloadable multimedia material available at http://ieeexplore.ieee.org provided by the authors. The Supplementary Material contains a video demonstration of surface mount LED integrated printed line under stretching, twisting, and crimping, as well as a file containing additional figures. This material is 18.5 MB in size.

Digital Object Identifier 10.1109/JSEN.2016.2605071

were studied [15]. This technique did not result in a crack formation, which is commonly encountered in metals upon elongation above 1%, due to the presence of alloy metal in liquid form at room temperature. Resistance change (ΔR) of 0.24 Ω with 100% strain was indicated, but lower stretchability ($\sim$30%) was observed when active circuit elements were integrated into liquid metal filled micro-channels. Furthermore, an in-plane metal conductor technology for horseshoe shaped meandering lines was proposed by [16] to pattern copper with a polyimide support underneath. The polyimide support layer increased the fatigue life (3,400 cycles at 10% strain) of the meandering line. The fatigue life was further increased to 40,000 cycles at 30% strain by the addition of a supporting polyimide layer on top of the copper layer [17].

More recently, notable research has been done in nanomaterial research and development to fabricate stretchable interconnects. Carbon nanotubes (CNTs) and carbon black (CB) filled elastomers were developed toward the fabrication of strain gauges [18]. It was shown that CB filled elastomers had ΔR/R of $\sim$140% at 5% strain because of separation of carbon particles with applied strain, which produced breakage of the conductive pathways. Likewise, serpentine shaped CNT filled elastomers had a ΔR/R of $\sim$5% at 15% strain due to rotation and slide of CNTs against each other upon applied strain. In another study [19], silver nanowires (AgNWs) and silver nanoparticles (AgNPs) embedded in an elastomeric matrix had ΔR/R of $\sim$2 after 1,000 cycles with 10% strain, which was attributed to AgNW breakage with high number of cycles. Even though some of the aforementioned methods and novel materials show excellent stretchability and endurance results, their manufacturing complexity, material cost, and scalability limit their usage in mass production of wearable electronics. For example, the current market price of CNTs and AgNWs is relatively expensive than conductive inks, which limits their usage to only nano-based applications rather than large-scale fabrications.

Other large-scale mass-production techniques such as knitting [20] and weaving [8] have been used in integration of electronic functionality into smart garments. Knitting polyurethane covered copper fibers with conventional yarns yielded 1% resistance change up to 300% strain values [21]. Screen-printing of the conductive inks, on the other hand, is an alternative industry scalable technique for fabrication of inexpensive electronic devices on various substrates (e.g., textiles, polymeric films). It does not involve material extraction and removal steps as commonly found in semiconductor fabrication processes. Printing of various silver inks has been investigated on polyarylate films [22], woven and knitted fabrics [23], and nonwoven fabrics [24]. However, the electromechanical properties of the printed lines as a function of stretching were not investigated. On the other hand, a brush painting of poly(3,4-ethylenedioxythiophene):poly(styrene sulfonate) (PEDOT:PSS) conducting polymer on knitted fabrics was studied [25], reporting an elastic stretchability up to 30%. The resistance change after 1000 stretching cycles with 20% strain was about 10%. Screen-printing of horseshoe shaped silver ink on TPU films was studied in [26], and 7% stretchability value was reported. Finally, another study [27] showed development and printing of a new ink material with stretchability of >93% and endurance of 1,000 cycles at 30% strain. However, the design and optimization of the printed conductive meandering lines on films, its subsequent integration onto textile wearables, and the effect of stretching on the electrical properties of the printed lines were not studied thoroughly before. Addressing these matters will shed light on some of the challenges (e.g. interconnect reliability under large strains, electronics integration, and washability) in textile-based electronics.

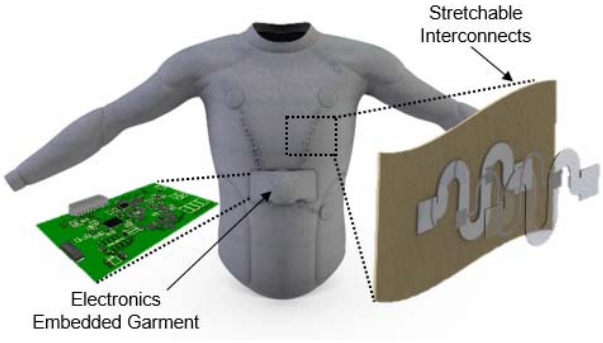

Fig. 1. Stretchable printed interconnect embedded smart garment being developed by ASSIST that incorporates low power electronics, sensors, and energy harvesting devices.

In this study, printed meandering interconnects were fabricated on knit fabrics. Inexpensive and scalable screen printing techniques were utilized to print Ag/AgCl conductive ink on thermoplastic polyurethane (TPU) film. Its heat lamination onto knit fabric and subsequent protective encapsulation layer yielded stretchable interconnects, shown Fig. 1. The printed stretchable interconnects are used in integration of low power sensors and energy harvesting devices developed by a National Science Foundation Nanosystems Engineering Research Center on Advanced Self-Powered Systems of Integrated Sensors and Technologies (ASSIST). This article focuses on the design and optimization of printed conductive meandering lines, as well as the effect of the processing steps on the electrical properties of the printed lines. Two demonstrations are provided to exemplify the use of the technique developed in this manuscript. First, a surface mount LED integration onto printed meandering lines as a means of evaluating the application of multi-electrode devices. Second, a shirt is modified with the meandering lines to support a full-signal electrocardiography measurement.

II. Stretchable Interconnects Fabrication

A. Screen-Printing of Stretchable Interconnects

Stretchable interconnects were printed on both knit fabric and thermoplastic polyurethane film (TPU). The knit fabric, acquired from Hanesbrands Inc., NC, USA, is made of 87% polyester and 13% spandex yarns with a basis weight of 150 g/m^2. Inclusion of spandex yarn within fabric construction yields high flexibility and recovery properties to the garment, which are important properties for intimate contact between the fabric and the diverse contours of the human body's surface. The TPU film (TL644), obtained from Bemis

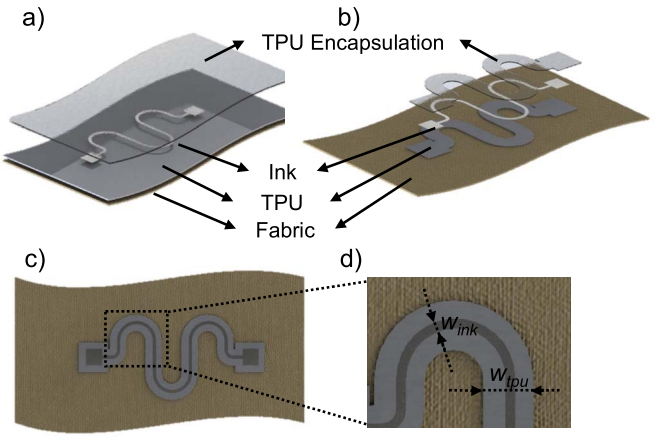

Fig. 2. Multilayer stretchable interconnect concept: (a) whole area TPU film lamination and TPU film encapsulation, (b) meandering shaped TPU film lamination and TPU film encapsulation, (c) top view of laminated and encapsulated structure, and (d) close-up picture of meandering line.

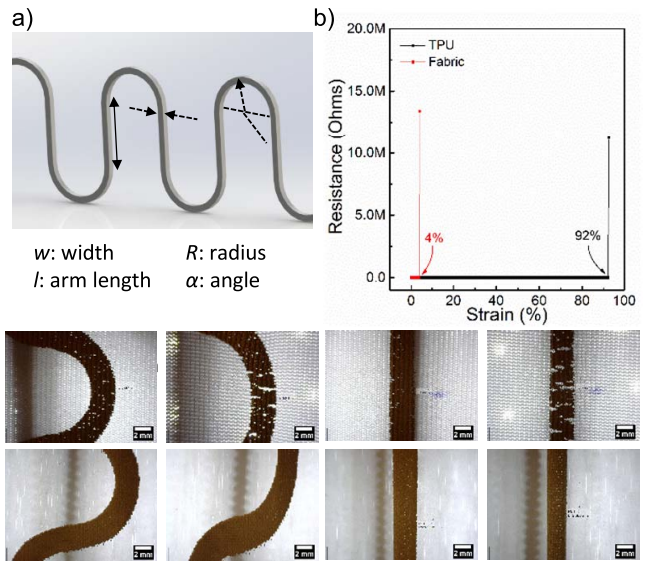

Fig. 3. (a) Meandering line design parameters (w, l, R, α), (b) resistance vs. strain behavior of the printed straight lines (width: 3mm, length: 14cm) on both knit fabric and TPU printing layer, (c), (d), (e), (f) digital microscope pictures of printed meandering and straight lines on knit fabric, and (g), (h), (i), (j) digital microscope pictures of printed meandering and straight lines on TPU printing layer.

Inc., MA, USA, is composed of two layers: a polymer film layer and an adhesive barrier layer. Because of the adhesive layer's low softening point (∼80 °C), the TPU film is suitable for heat sensitive fabrics during heat lamination. The film's ink receptive surface is suitable for screen-printing processes. It also has high washing resistance up to 60 °C. Creative Materials Ag/AgCl electrically conductive ink (product number: 124-36) was used for printing of stretchable interconnects on the TPU film and the knit fabric. The conductive ink shows excellent adhesion to a variety of substrates and has sufficient resistance to flexing and creasing.

The conductive ink printing was performed by using hand operated lab scale screen-printing equipment. A CAD drawn interconnect design was patterned onto a vinyl stencil by using a Silhouette cameo die cutter. The adhesive stencil was then placed onto a 100-mesh size screen-printing frame, and the ink was transferred onto the substrates by a hand-held squeegee at a 45° angle with operator controlled pressure.

B. Multi-Layer Stretchable Interconnects

The presented multilayer stretchable interconnect structure is given in Fig 2. The layered structure is composed of four layers. The knit fabric (thickness: 0.46 mm) lies at the bottom, representing the garment. The TPU film (TL644, thickness: 0.1 mm), the meandering shaped conductive ink layer, and the TPU encapsulation (TL3916, Bemis Inc., thickness: 0.15 mm) are situated on top of the knitted fabric, respectively. The TPU film (TL644) and the TPU encapsulation film (TL3916) will be referred as printing layer and encapsulation layer, respectively, for the rest of the study. Fig. 2(a) shows the layered structure where the dimensions of the knitted fabric, the printing layer, and the encapsulation layer are similar (6 cm × 16 cm). Whereas, in Fig. 2(b) the printing layer and encapsulation layer are cut to a meandering shape and then laminated on top of similar size knit fabric. Fig. 2(c) and 2(d) display the top view of the layered structure. The width of printed ink and the encapsulation layer are shown as w_{ink} and w_{tpu}, respectively. The printing layer and the encapsulation layer widths are the same, defined by an offset from the edge of the ink width, $w_{offset} = (w_{tpu}\text{-}w_{ink})/2$. The stretchable interconnect fabrication steps in Fig. 2(a) are given below.

1) Cut a 6 cm × 16 cm knitted fabric in warp direction.
2) Cut a 6 cm × 16 cm TPU film (TL644) for printing layer.
3) Screen-print conductive ink on the printing side (non-adhesive side) of the printing layer (2 passes of conductive ink) and cure at 60 °C for 15 min.
4) Laminate conductive ink printed layer onto knitted fabric with a heat press at 125 °C for 2 min.
5) Laminate the encapsulation layer on top of the printed line at 125 °C for 2 min.

The multilayer interconnect structure in Fig. 2(b) was also fabricated by cutting of the printing and encapsulation layers with w_{offset} values of 2 mm and 4 mm. The rest of the procedure is similar as given for Fig. 2(a).

III. Results and Discussion

A. Screen-Printing of Conductive Ink on Knitted Fabric and TPU Film

Meandering and straight lines were initially printed on both the knit fabric and the TPU film individually without any lamination and encapsulation steps. The design of the meandering line is given in Fig. 3(a). The design was determined by the parameters: width (w), arm length (l), radius (R), and angle (α). A straight line with a 3 mm width and 14 cm length, and a meandering line ($w = 3$ mm, $l = 0$ mm, $R = 5$ mm, $\alpha = 0°$ and total length=13.4 cm) were printed on both substrates. Their surface topology and electromechanical properties were compared. The surface properties of the printed ink were analyzed by Scanning Electron Microscopy (SEM), Optical Microscopy, and Digital Microscope and Atomic Force Microscope (AFM). The in-situ

electromechanical properties of the printed lines were measured with a MTS tensile tester (gauge length: 11.5 cm, crosshead speed: 5 cm/min). Two-probe electrical resistance was simultaneously recorded (2 Hz) with LabVIEW software. Fig. 3(b) shows the resistance change of the printed straight traces on the knit fabric and the TPU film as the samples were elongated. The printed straight lines failed (open electrical resistance) at $2.16\% \pm 2.60\%$ strain on the knit fabric. However, the same printed line on the TPU film could withstand up to $98.60\% \pm 9.02\%$ strain. On the other hand, the meandering lines on the knit fabric and the TPU film were able to be stretched up to $34.85\% \pm 0.64\%$ and $112.84\% \pm 23.67\%$ strains, respectively, without electrical failure. The digital microscopy pictures of the printed meandering and straight lines on the knitted fabric and the TPU film are given in Fig. 3(c)-(f) and Fig. 3(g)-(j). The pictures were taken with a digital microscope situated over a custom-built stretching device strained the sample in discrete strain intervals. The printed straight and meandering lines on the knit fabric showed significant crack formation at 40% strain, relative to that on the TPU film. This result can be attributed to the high surface roughness and surface area of the knit fabric compared to the TPU film. Two passes of conductive ink printing on the knitted fabric created less surface coating due to its high fibrous surface area. Uncoated areas were still visible on the surface of the knitted fabric after the screen-printing process in Fig. 3(c) and 3(e). The printed ink penetrates through the structure of the yarn. It also fills the large gaps that are created by the inter-looped formation during knitting process. Therefore, the same amount of ink on the knitted fabric yielded less continuous conductive tracks, which made it sensitive to stretching at low strain values. The conductive ink printing on the TPU film yielded had a thickness of 20 micrometers, as shown in Fig 4(b). Inspection did show localized sections of the meandering line to be as high as 50 micrometers. The variability in the thickness of the ink is much lower as compared to ink printed on fabrics. This was due to the TPU film's relatively smooth surface (Fig. 4(a) and 4(c)) compared to the knitted fabric surface. This was shown with an AFM surface topology picture (Fig. 4(d)). The TPU film had a roughness value of 0.185 micrometers, which yielded a continuous formation of conductive tracks on TPU surface. Thus, the straight and meandering lines on TPU film at 40% strain had less visible holes and crack formation relative to that on the knit fabric. Due to strain relief property of the meandering line, the maximum stretchability of the meandering line on both substrates was higher than that of the straight line.

To investigate the relationship of resistance change vs. meandering line design parameters (i.e., width (ω), arm length (l), radius (R), angle (α)), different meandering lines were printed on the TPU printing layer (without lamination on the knit fabric and TPU encapsulation), and a final meandering line type was selected in the end to further study in the following sections. The meandering line design parameters along with digital pictures of the printed lines are given in Fig. 1, Fig. 2 and Fig. 3 in Supplementary Information section. Similar constant strain rate electromechanical tests

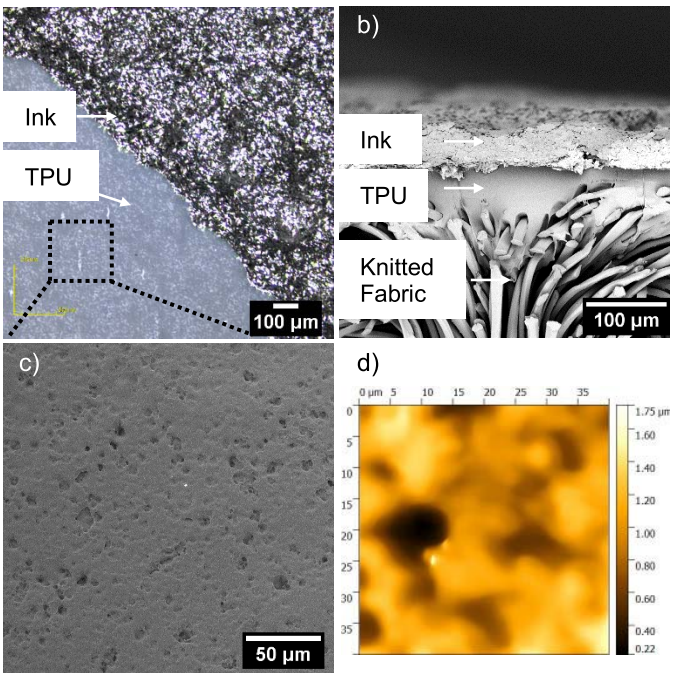

Fig. 4. (a) Optical microscopy picture of the ink on TPU film. (b) SEM cross-sectional picture of the printed conductive ink on TPU film. (c) SEM surface picture of the TPU film. (d) AFM surface topology of the TPU printing layer.

were performed on the samples as was previously mentioned. The comparison of different meandering line types was made based upon $\Delta R/R$ values at 40% strains, which were obtained as a result of in-situ electromechanical tests. The results are shown in Fig. 5a. The figure shows $\Delta R/R$ vs. strain up to 40% applied strain. Each printed blocks were located on the perimeter of the plot according to decreasing $\Delta R/R$ value. The inner curves correspond to the applied strains of 10, 20, 30, 40%. Blocks A1 through A5 represent $w = 1$ to 5 mm, $l = 0$ mm, $R = 5$ mm, and $\alpha = 0°$ (width varies). Blocks B1 through B5 represent $w = 1$ to 5 mm, $l = 5$ mm, $R = 5$ mm, and $\alpha = 0°$ (width varies). Blocks C1 through C3 show $w = 1$'mm, $l = 5$, 10, 15 mm, $R = 5$ mm, and $\alpha = 0°$ (arm length varies). Blocks D1 through D4 denote $w = 1$ mm, $l = 0$ mm, $R = 5$ mm, and $\alpha = -20$, 20, 30, 45° (angle varies), and blocks E1 through E3 indicate $w = 1$ mm, $l = 5$ mm, $R = 5$ mm, and $\alpha = -20$, 0, 20° (angle varies). Total of 20 blocks were printed (three replications for each block). The dimensions of each block were tabulated in Supplementary Information section. In blocks A1-A5 and B1-B5, increasing the width (ω) of the printed line decreased the value of $\Delta R/R$. This might be attributed to crack formation and propagation across the width of the crest region of the meandering line, which might be the predominant effect in meandering lines with small width values. In blocks C1-C3, increasing the arm length (l) decreased the value of $\Delta R/R$. In blocks D1-D4, increasing the angle (α) gave a decreasing trend in $\Delta R/R$. For the blocks E1-E3, decreasing the angle (α) yielded a decreasing trend in $\Delta R/R$ values. The printed lines (blocks: A5, B3, D3) did not follow the trend as it can be seen from Fig. 5(a), which may be ascribed to uneven coating of the TPU film surface due to the variations in the

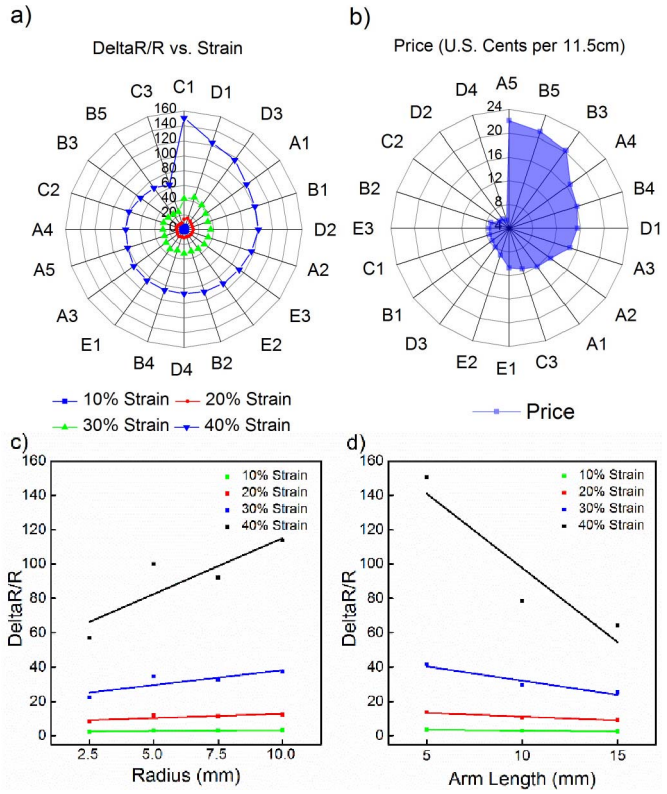

Fig. 5. (a) ΔR/R vs. strain as a function of printed meandering line parameters (w, l, R, α). (b) Price of corresponding printed blocks. (c) ΔR/R vs. radius of block C2 at different strain values. (d) ΔR/R vs. arm length of block C2 at different strain values.

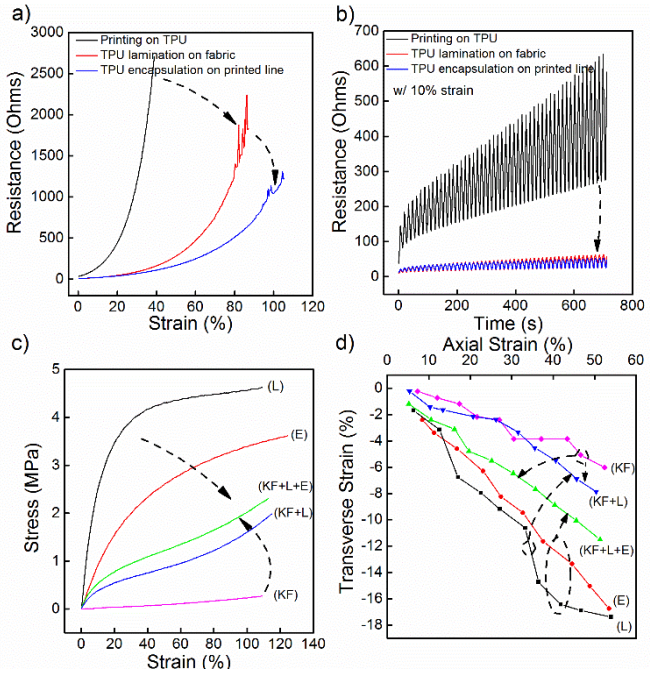

Fig. 6. (a) One-time stretching test of each fabrication step samples (test speed: 5.08 cm/min). (b) Cycling test of each fabrication step samples (test speed: 10.16 cm/min). (c)Mechanical properties of constituents of multilayer structure. (d)Transverse contraction of the constituent layers and the final multilayer structure with axial strain.

screen-printing process. While finite element analysis (FEA) might be required to validate and compare the induced strain and stress on the printed lines and also the change in ΔR/R as a function of meandering line parameters, it is noted that a goal in this work is to evaluate the techno-economic performance of the patterned structures, ideally choosing a meandering line design that has a combination of high performance and low cost. The blocks C2, B3, B5, and C3 had the lowest ΔR/R among the printed blocks (78.5, 73.1, 69.7, and 64.1 Ω, respectively). Fig. 5(b) shows the price of each printed block per gauge length (11.5 cm) in tensile testing. The equivalent line length for each block type was calculated according to the resistance formula (R= ρL/wt). Averaged measured resistance (R, number of samples=3), resistivity (ρ) of 0.0002 Ω-cm, thickness (t) of 20 μm and printed width (w) were utilized in the calculation. Finally, the printing cost was calculated and plotted by finding the averaged ink amount (N=3) for a length of 11.5 cm and then multiplying it with the ink's cost ($4/g). Localized variation in these dimensions can expect to induce some uncertainty in the cost calculation. These effects would be two-fold. Increasing the thickness of the conductive layer would decrease the resistance of the line due to addition of more conductive material per unit length. The increased thickness would also increase materials usage and raise the cost of the printing. For the parameters used in this analysis, blocks E4, C2, D2, and D4 had the cheapest printing cost among the printed blocks (6.60, 6.00, 5.95, 5.43 cents, respectively). The block C2 was selected for further testing in following sections since its cost was much lower than blocks B5 and B3 (20 and 21 cents). Also, block C2 was less wide than the block C3 (22 mm vs. 27 mm). This architecture also occupies less printing space, thus enabling the potential for a higher density of printed interconnects.

B. Lamination of TPU Printing Layer on Knit Fabric and Encapsulation of Conductive Ink

The selected block C2 meandering line shape (w = 1 mm, l = 5 mm, R = 5 mm, α = 0°) in Section III-A was used in this section. The fabrication procedure in Fig. 2(a) was followed as described in Section II-B. The meandering line was screen-printed onto the TPU printing layer (rectangular, 6 cm × 16 cm). It was then laminated on the knit fabric. Afterwards, it was covered with a TPU film encapsulation (rectangular, 6 cm × 16 cm). Heat laminated TPU film layer provides insulation and protects the printed lines from mechanical and environmental damage as other silicone and acrylic encapsulation coatings [23], [24]. In addition, it eliminates additional screen preparation and cleaning steps in screen-printing process. Optical microscopy and SEM cross-sectional pictures of the final multilayer structure are given in Fig. 7(a) and 7(b). Mechanical properties of each layer are given in Fig. 6(c) and 6(d). The TPU printing layer, the TPU encapsulation layer, and the knit fabric are denoted as L, E, and KF, respectively. Lamination of TPU printing layer on knit fabric is denoted as KF+L, and the combination of all of the layers is shown as KF+L+E. Fig. 6(c) shows the stress vs. strain graph of each layer and the final laminated multilayer structure. Young's modulus (modulus=stress/strain, calculated

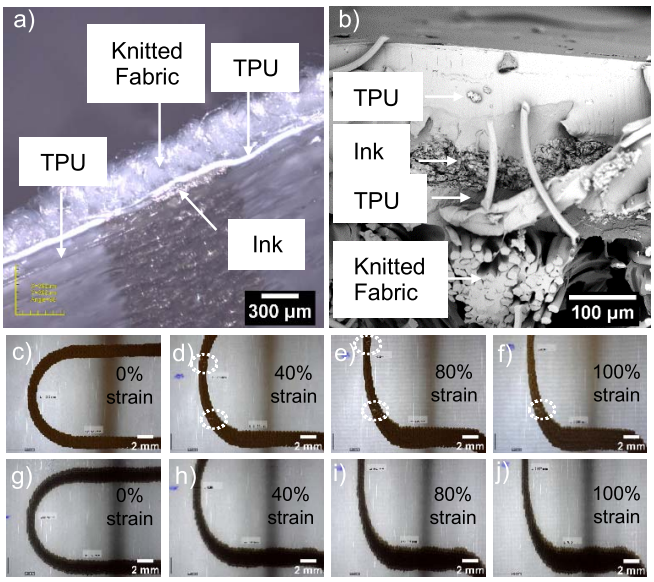

Fig. 7. (a) Optical picture of TPU laminated and encapsulated multilayer stretchable interconnect structure. (b) SEM cross-sectional view of multilayer stretchable interconnect structure. (c)–(f) Digital microscope pictures with stretching of TPU film laminated knit fabric. (g)–(j) Digital microscope pictures with stretching when TPU encapsulation layer was added on the printed line.

at 10% strain) of the printing layer (L), the encapsulation layer (E), and the knit fabric was calculated as 248, 90, and 1.4 kPa, respectively. The Young's modulus for KF+L and KF+L+E were found as 37 kPa and 52 kPa. Addition of the individual layers created a new multilayer structure whose mechanical properties fall between the mechanical properties of the individual layers. Fig. 6(d) describes how much transverse contraction occurs with an axial strain (i.e., Poisson's ratio=-transverse contraction/axial strain). The Poisson's ratios for L, E, KF+L+E, KF+L, and KF were calculated from the slope of the curves as 0.4, 0.3, 0.22, 0.14, and 0.09, respectively. Similar to the Young's modulus, Poisson's ratio for the multilayer structure falls between Poisson's ratio of the constituent layers.

To investigate the effect of each step (lamination and encapsulation) on the electrical properties of the printed line, one-time in-situ stretching tensile test and cyclic tensile test were performed. The results are presented in Fig. 6(a) and 6(b). Fig. 6(a) shows the resistance change vs. strain for the test sample as it goes through each fabrication step. Block C2 printed TPU film had the sharpest strain change with strain, and its electrical failure was at $52.47\% \pm 8.28\%$ strain. When the printed layer was laminated on the knit fabric, the failure strain went up to $78.82\% \pm 11.68\%$. As the TPU encapsulation layer was applied to the rest of the layered structure, the failure strain value went up to $103.91\% \pm 5.31\%$. The cyclic tensile test results (10% strain and 100 cycles) of each fabrication step are shown in Fig. 6(b). The block C2 printed TPU film had the highest resistance change when the number of cycles increased. The cyclic tensile testing of the multilayer structure before and after the encapsulation layer had a very slight difference. The increase in stretchability in the one-time stretching test and cyclic tensile test was attributed to both lamination temperature and TPU encapsulation. The TPU film lamination and TPU encapsulation process temperatures (125 °C) were higher than the ink curing temperature (60 °C). Thus, this resulted in a resistance drop of about 70% in the ink. Since the TPU encapsulation layer enclosed the ink on the topside, an improvement in one time stretching and cyclic tensile testing properties was observed due to the retardation of deformation of the ink layer. The encapsulation layer inhibited significant crack formation with extension and helped to recover the ink layer to its initial state. Improvement of the results in Fig. 6(a) and 6(b) can be explained by investigation of the microstructure of the ink as it is strained. Fig. 7(c)-7(f) shows the crack formation on the printed line with strain for the printing layer laminated knit fabric sample. The visible cracks (encircled) were observed on the crest region of the meandering line starting at 20% strain and on. However, no visible cracks were found after TPU film encapsulation on the printed line in Fig. 7(g)-7(j). This explained the early resistance increase in low stain values in Fig. 7(a). When the sample was uniaxially stretched, the width of the arm region of the meandering line increased, and the crest region of the meandering line was narrowed and elongated. In contrast, the length of crest region of the meandering line extended, and its peak width decreased. To investigate which region of the meandering line (crest vs. arm) had the most effect on the $\Delta R/R$ value, the C2 blocks with various radii ($R = 2.5$, 5, 7.5, and 10 mm) and arm length values ($l = 5$, 10, and 15 mm) were printed on the TPU film. It is helpful to note that an increased radius corresponds to increased crest length of the printed line (perimeter of crest region=$2\pi R$). The results are given in Fig. 5(c) and 5(d). Fig. 5(c) shows $\Delta R/R$ vs. radius change at different strain values. As the radius of the meandering line was increased, the deformation in the printed line increased. This testing scenario corresponds to the stretched sample conditions in Fig. 7(c)-7(j). The meandering line's crest region length increases with stretching, thus, the deformation ($\Delta R/R$) of the printed line increases. Increasing the arm length decreased the deformation in the meandering line, shown in Fig. 5(d). However, when the sample was stretched in Fig. 7(g)-7(j), the arm length did not change (its width was widened). Therefore, it was concluded that the crest region was the region resulting in a significant resistance increase as the sample was elongated.

Thus far, only rectangular cut (6 cm × 16 cm) samples of the printing layer and encapsulation layer lamination onto knitted fabric were presented, shown in Fig. 2(a). The effect of removing excess TPU printing layer and encapsulation layer on the electrical properties of the printed interconnects is studied from now on, shown in Fig. 2b. A similar fabrication procedure was followed as described in Section II-B except the dimensions of the TPU printing layer and TPU encapsulation layer were determined by offsetting the printed block C2 meandering design by amount of w_{offset}, as shown in Fig. 2(d). Two offset values (2 mm and 4 mm) were tested. Similar one-time stretching and cyclic tensile tests were performed to explore the effect of removing extra material from the printing and encapsulation layers. Fig. 8(a) and 8(b) shows the cycling testing (10% strain and 100 cycles) results of whole area (rectangular) vs. 2 mm offset cut (meandering shaped

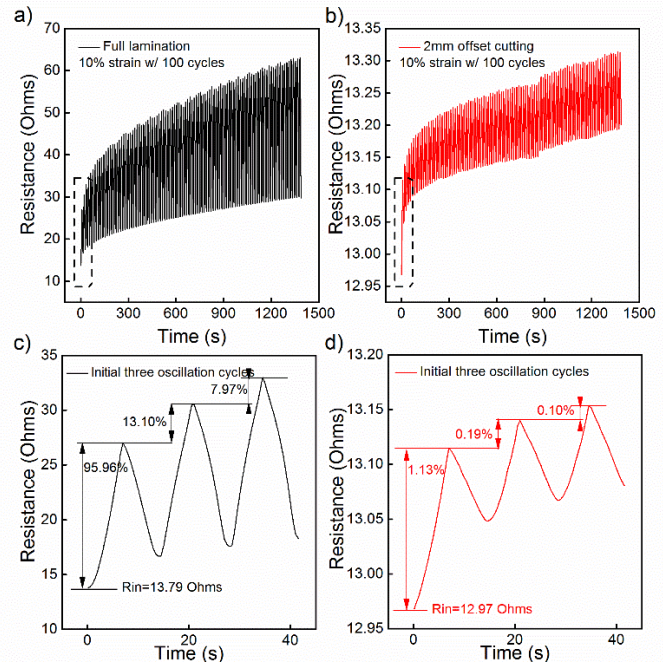

Fig. 8. Cycling test of multilayer interconnect structure (test speed: 10.16 cm/min), (a) whole area TPU lamination and encapsulation, (b) meandering line shaped (offset-cut) TPU lamination and encapsulation, (c) initial three cycles of Fig. 8(a), and (d) initial three cycles of Fig. 8(b).

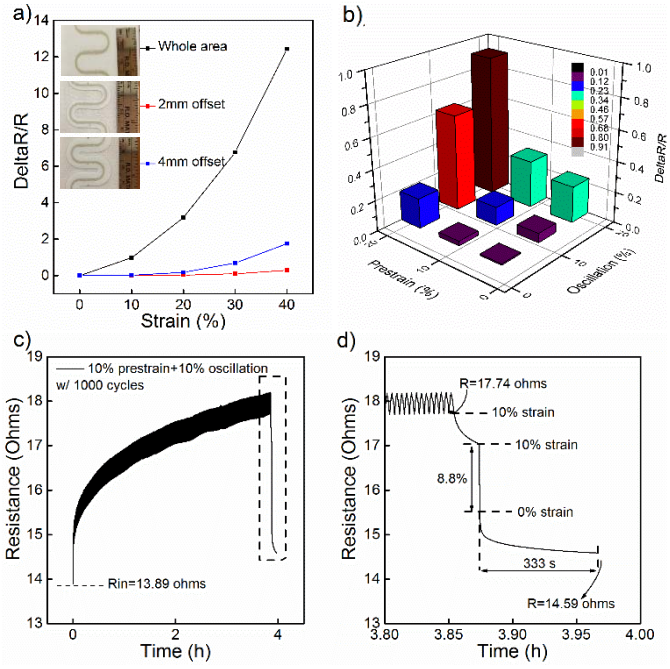

Fig. 9. (a) One-time stretching test of whole area TPU lamination vs. 2 mm and 4mm offset meandering shaped TPU lamination (test speed: 5.08 cm/min). (b) ΔR/R vs. discrete pre-strain and cyclic tensile strains (test speed: 10.16 cm/min). (c) 1000 cycle cycling test with 10% prestrain and succeeding 10% cycling strain (test speed: 10.16 cm/min). (d) Zoom-out region of the marked region in Fig. 9(c).

TPU layer) multilayer structure. The latter had only 0.23 Ω resistance change at the end of 100 cycles, whereas, the rectangular cut lamination had a resistance change of 16.37 Ω. The first three oscillation cycles of Fig. 8(a) and 8(b) are given in Fig. 8(c) and 8(d). In Fig. 8(c), an initial straining of the sample by 10% resulted in a resistance increase of 95.96%, and the subsequent second and third cycles had a percent resistance increase of 13.10% and 7.97%. The percent resistance change trend decreased with succeeding stretching cycles (i.e., less deformation in the ink with succeeding cycles). In contrast, the percent resistance increase in Fig. 8(d) was only 1.13%, and the following cycles had 0.19% and 0.1% resistance increase. For the meandering shaped multilayer interconnect (Fig. 2(b)), the applied strain resulted in extension of the knit fabric between the printed meandering lines, where there was no lamination of TPU film. This part of the fabric underwent more straining without imposing more strain on the ink, which produced high flexibility while minimizing resistance change with strain. One-time stretching results are shown in Fig. 9(a) up to 40% strain. The inset image in Fig. 9(a) shows the pictures of the fabricated samples. The 2 mm offset cut sample showed the smallest resistance change (ΔR/R=0.29) at 40% strain. The 4 mm offset and full area laminated multilayer interconnects had ΔR/R values of 1.75 and 12.43, respectively. Removing the excess material resulted in less strain in the ink layer, which contributed to smaller resistance change upon elongation. The removal of TPU layers between two subsequent arms of printed meandering lines yielded larger strain values for a constant ΔR/R value compared to whole area rectangular lamination.

To simulate the daily use of the garment (i.e., straining during dressing and additional strains due to body movement), the multilayer stretchable printed line structure (Fig. 2(b), w_{offset} = 2 mm) was exposed to various pre-strain and cyclic strains in cyclic tensile testing. In other words, the test sample was pre-strained by a certain amount on tensile testing equipment, and then subsequent 100 cycles were applied with an additional cyclic tensile strain. The pre-strain and cyclic tensile strain values were selected as 5%, 10%, and 20%. The result is given in Fig. 9b. At a constant pre-strain value, increasing the cyclic strain value increased the ΔR/R. Similar increasing trend in ΔR/R was obtained for increasing pre-strain value at constant cyclic tensile strain. The lowest ΔR/R value calculated was with 5% pre-strain + 5% cyclic tensile strain (ΔR/R=0.009). The highest ΔR/R value was with 20% pre-strain + 20% cyclic strain (ΔR/R=0.91), as expected. Higher total strain (pre-strain+cyclic strain) led to increased deformation in the printed line. To further investigate electrical properties of the stretchable meandering printed lines a 1,000 cycles were performed on the cyclic tensile test with a 10% pre-strain + 10% cyclic strain. The results of the test are given in Fig. 9(c) and 9(d). The resistance curve slightly levels off over time in Fig. 9(c). This was attributed to the decreasing percent resistance change of the printed line with an increasing number of cycles, as explained in Fig. 8(d). The printed line resistance changed only by 3.85 Ω at the end of 1,000 cycles, shown in Fig. 9(d). When the tensile tester crosshead was brought down from 10% strain to 0% strain, the recovery in the resistance was 8.8%. At 0% strain, the resistance of the sample decreased exponentially over time due to the recovery of ink and the multilayer substrate. The resistance value was 14.59 Ω after 333 seconds. This value

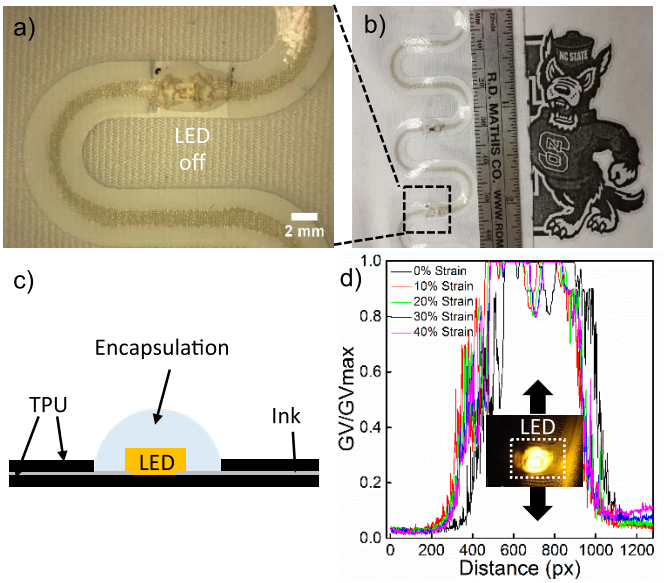

Fig. 10. (a) Close up picture of LED integrated printed stretchable line. (b) LED integrated stretchable line. (c) Cross-sectional view of LED integration. (d) LED intensity with stretching. Inset: Stretched LED integrated printed line.

could further decrease over time if the decreasing slope of the resistance was taken into account in the rectangular marked area in Fig. 9(c). It is important to reiterate that the testing in Fig. 9(c) and 9(d) mimics a real human scenario, where the pre-strain is the initial strain generated on the printed line when a garment is placed on the body. This is followed by a cyclic strain that simulates the daily use of the garment. The self-healing of the resistance at the end of the test replicates the garment removal and storage.

C. Washing Durability and Stretchable Interconnects Demonstrations

An accelerated wash test (AATCC 61-2a) was performed to examine the effectiveness of the TPU encapsulation on the ink's electrical performance. One accelerated wash test is equivalent to 5 home launderings. A total of six samples with and without TPU encapsulation were fabricated according to the procedure in Fig. 2(a). The samples were placed into metal containers with 50 steel spheres and washed at 49 °C with a powder detergent. The samples without TPU encapsulation were not conductive after initial 5 home washing cycles. However, the samples with the TPU encapsulation ($R_{initial}$ = 7.45 Ω ± 1.73 Ω) were still conductive after 100 washing cycles with a resistance increase of 4.6 Ω.

To demonstrate this technology, a surface mount LED was integrated on the stretchable printed line with a 51 Ω surface mount resistor to show the applicability and use of the proposed stretchable printed meandering lines, shown in Fig. 10(a) and 10(b). The LED was bonded to conductive traces by using silver epoxy (CircuitWorks 2400). It was then encapsulated with UV curable encapsulant (Dymax 9001) to give mechanical stiffening and eliminate debonding of LED. The cross-sectional image of its integration is shown in Fig. 10(c). The integrated LED was powered with a 3V coin cell battery. Afterwards, the LED integrated printed line

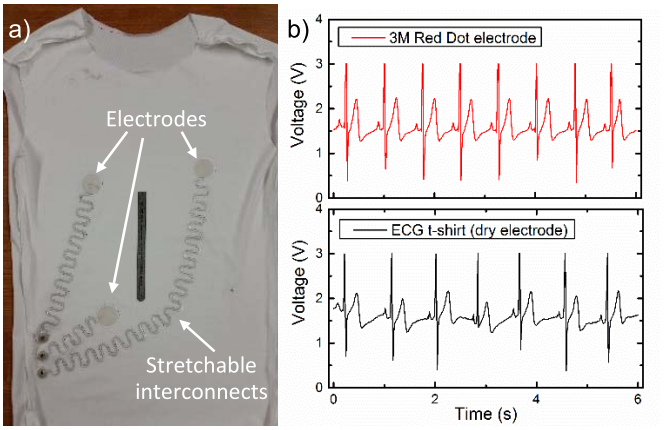

Fig. 11. (a) Inner side of the fabricated ECG t-shirt. (b) Recorded ECG signals from 3M Red Dot electrode and ECG t-shirt.

was stretched up 100% strain with a custom-built straining device, and simultaneously the surface picture was taken with a digital microscope in a dark room. The recorded video of the integrated LED was provided in the Supplementary Information section. The LED light turned off above 80% strain due to the resistance increase in the printed line, which decreased the voltage drop across the LED. However, the LED light turned back on with the recovery of the printed line. The LED light intensity up to 40% strain is given in Fig. 10(d). The intensity plot was obtained by image processing of the captured image in MATLAB software. The vertical axis represents normalized grayscale value (GV/GV_{max}). It was observed that the light intensity did not change up to 40% strain. However, a horizontal shift was observed in the graph due to out-of-plane rotation of the LED during stretching.

For a second demonstration, an electrocardiography (ECG) shirt was fabricated to show the use of fabricated stretchable printed lines to monitor the electrical activity of the heart. Fig. 11(a) shows the inner side of the t-shirt, where three 30 mm printed dry electrodes [28] were printed along with stretchable meandering lines. The distance between electrode pairs was kept at 13 cm. Lead I of Einthoven's triangle configuration was used to measure the potential difference between electrode pairs. ECG measurement was made with a Vernier ECG signal acquisition device (1 V/1 mV gain, sampling rate: 100 Hz). A healthy male subject wore the fabricated t-shirt, and an ECG measurement was taken while the subject was standing. Fig. 11(b) shows the recorded ECG signals with 3M Red Dot electrode (as reference) and with the ECG shirt. The acquired ECG signals show comparable ECG signals with characteristic PQRST electrocardiogram peaks.

IV. Conclusion

A multilayer stretchable interconnect design was fabricated by screen-printing Ag/AgCl ink on thermoplastic polyurethane (TPU) film. Its subsequent heat lamination onto a knit fabric, and a TPU encapsulation on the ink layer yielded a novel multilayer stretchable interconnect structure.

Printing the meandering and straight line on the TPU film layer provided high failure strain values compared to the knit

fabric alone. A set of design of experiments was conducted to determine the most suitable meandering line by changing the meandering line parameters (width, arm length, radius, and angle). Block C2 ($w = 1$ mm, $l = 5$ mm, $R = 5$ mm, $\alpha = 0°$) was chosen due to its low ΔR/R value and inexpensive printing cost.

Lamination of the printing layer on the knit fabric and encapsulation of the ink layer with TPU film were explored. The conductive ink printed TPU layer with a knit fabric backing decreased deformation on the ink. Moreover, the TPU film encapsulation on the ink layer prevented the ink from significantly cracking and helped to recover the ink to its initial position.

The effect of decreasing the area and shape of the printing and encapsulation layer was investigated. It was found that the meandering shaped printing and encapsulation layers significantly decreased the resistance change in one time stretching and cycling tests. The multilayer meandering shaped structure was cycled 1,000 times in a simulation of a human use scenario, and only 0.7 Ω resistance change was observed. In our study, the maximum stretchability achieved was about 110% with the 2 mm offset sample. Materials factors of the ink not considered in this work such as chemical and physical properties of the polymer, solvent and surfactant type, and filler type and its concentration provide additional opportunities for improved performance. In addition, synergy of novel elastic ink chemistries with strain-relief printed line designs may yield higher stretchability values.

Finally, a surface mount LED integration on stretchable printed lines and an ECG shirt with meandering lines were demonstrated. The integrated LED was resistant to stretching, flexing and twisting, which might be used in wearable optical based sensors. Moreover, the ECG shirt acquired similar ECG signals compared to the reference electrodes. The proposed inexpensive and washable (100 wash cycles) multilayer interconnects design has utmost importance in integration of sensors, antennas, and energy harvesting devices on garments for wearable electronics.

ACKNOWLEDGMENT

The authors would like to thank J. Halbur from North Carolina State University for his help on LabVIEW programming for the resistance measurement.

REFERENCES

[1] M. Ciocchetti *et al.*, "Smart Textile based on fiber bragg grating sensors for respiratory monitoring: Design and preliminary trials," *Biosensors*, vol. 5, no. 3, pp. 602–615, Sep. 2015.

[2] F. M. Kelly, L. Meunier, C. Cochrane, and V. Koncar, "Polyaniline: Application as solid state electrochromic in a flexible textile display," *Displays*, vol. 34, no. 1, pp. 1–7, Jan. 2013.

[3] Q. He *et al.*, "Fabrication of flexible MoS_2 thin-film transistor arrays for practical gas-sensing applications," *Small*, vol. 8, no. 19, pp. 2994–2999, Oct. 2012.

[4] Y. He *et al.*, "Freestanding three-dimensional graphene/MnO_2 Composite networks as ultralight and flexible supercapacitor electrodes," *ACS Nano*, vol. 7, no. 1, pp. 174–182, Dec. 2012.

[5] Y. Cheng, R. Wang, J. Sun, and L. Gao, "Highly conductive and ultrastretchable electric circuits from covered yarns and silver nanowires," *ACS Nano*, vol. 9, no. 4, pp. 3887–3895, Mar. 2015.

[6] X. Pu *et al.*, "A self-charging power unit by integration of a textile triboelectric nanogenerator and a flexible lithium-ion battery for wearable electronics," *Adv. Mater.*, vol. 27, no. 15, pp. 2472–2478, Apr. 2015.

[7] C. Mattmann, O. Amft, H. Harms, G. Troster, and F. Clemens, "recognizing upper body postures using textile strain sensors," in *Proc. 11th IEEE Int. Symp. Wearable Comput.*, Oct. 2007, pp. 29–36.

[8] K. Cherenack, C. Zysset, T. Kinkeldei, N. Münzenrieder, and G. Tröster, "Woven electronic fibers with sensing and display functions for smart textiles," *Adv. Mater.*, vol. 22, no. 45, pp. 5178–5182, Dec. 2010.

[9] Y. Sun and J. A. Rogers, "Structural forms of single crystal semiconductor nanoribbons for high-performance stretchable electronics," *J. Mater. Chem.*, vol. 17, no. 9, pp. 832–840, Jan. 2007.

[10] S. P. Lacour, S. Wagner, Z. Huang, and Z. Suo, "Stretchable gold conductors on elastomeric substrates," *Appl. Phys. Lett.*, vol. 82, no. 15, pp. 2404–2406, 2003.

[11] T. Someya *et al.*, "Conformable, flexible, large-area networks of pressure and thermal sensors with organic transistor active matrixes," *Proc. Nat. Acad. Sci. USA*, vol. 102, no. 35, pp. 12321–12325, 2005.

[12] H. C. Ko *et al.*, "A hemispherical electronic eye camera based on compressible silicon optoelectronics," *Nature*, vol. 454, pp. 748–753, Aug. 2008.

[13] D. S. Gray, J. Tien, and C. S. Chen, "High-conductivity elastomeric electronics," *Adv. Mater.*, vol. 16, no. 5, pp. 393–397, Mar. 2004.

[14] K. L. Lin and K. Jain, "Design and fabrication of stretchable multilayer self-aligned interconnects for flexible electronics and large-area sensor arrays using excimer laser photoablation," *IEEE Electron Device Lett.*, vol. 30, no. 1, pp. 14–17, Jan. 2009.

[15] H.-J. Kim, C. Son, and B. Ziaie, "A multiaxial stretchable interconnect using liquid-alloy-filled elastomeric microchannels," *Appl. Phys. Lett.*, vol. 92, no. 1, p. 011904, Jan. 2008.

[16] F. Bossuyt, T. Vervust, and J. Vanfleteren, "Stretchable electronics technology for large area applications: Fabrication and mechanical characterization," *IEEE Trans. Compon. Packag. Manuf. Technol.*, vol. 3, no. 2, pp. 229–235, Feb. 2013.

[17] Y. Y. Hsu, M. Gonzalez, F. Bossuyt, J. Vanfleteren, and I. D. Wolf, "Polyimide-enhanced stretchable interconnects: Design, fabrication, and characterization," *IEEE Trans. Electron Devices*, vol. 58, no. 8, pp. 2680–2688, Aug. 2011.

[18] N. Lu, C. Lu, S. Yang, and J. Rogers, "Highly sensitive skin-mountable strain gauges based entirely on elastomers," *Adv. Funct. Mater.*, vol. 22, no. 19, pp. 4044–4050, 2012.

[19] S. Lee *et al.*, "Ag nanowire reinforced highly stretchable conductive fibers for wearable electronics," *Adv. Funct. Mater.*, vol. 25, no. 21, pp. 3114–3121, Jun. 2015.

[20] Q. Li and X. Tao, "A stretchable knitted interconnect for three-dimensional curvilinear surfaces," *Textile Res. J.*, vol. 81, no. 11, pp. 1171–1182, Jul. 2011.

[21] Q. Li and X. M. Tao, "Three-dimensionally deformable, highly stretchable, permeable, durable and washable fabric circuit boards," *Proc. Roy. Soc. London Math. Phys. Eng. Sci.*, vol. 470, no. 2171, p. 20140472, Nov. 2014.

[22] T. H. J. van Osch, J. Perelaer, A. W. M. de Laat, and U. S. Schubert, "Inkjet printing of narrow conductive tracks on untreated polymeric substrates," *Adv. Mater.*, vol. 20, no. 2, pp. 343–345, Jan. 2008.

[23] M. Suh, K. E. Carroll, E. Grant, and W. Oxenham, "Effect of fabric substrate and coating material on the quality of conductive printing," *J. Textile Inst.*, vol. 104, no. 2, pp. 213–222, Feb. 2013.

[24] B. Karaguzel *et al.*, "Flexible, durable printed electrical circuits," *J. Textile Inst.*, vol. 100, no. 1, pp. 1–9, Mar. 2009.

[25] S. Takamatsu, T. Lonjaret, E. Ismailova, A. Masuda, T. Itoh, and G. G. Malliaras, "Wearable keyboard using conducting polymer electrodes on textiles,"*Adv. Mater.*, vol. 28, no. 22, pp. 4485–4488, Jun. 2015.

[26] K.-S. Kim, K.-H. Jung, and S.-B. Jung, "Design and fabrication of screen-printed silver circuits for stretchable electronics," *Microelectron. Eng.*, vol. 120, pp. 216–220, May 2014.

[27] N. Matsuhisa *et al.*, "Printable elastic conductors with a high conductivity for electronic textile applications," *Nat. Commun.*, vol. 6, p. 7461, Jun. 2015.

[28] M. A. Yokus and J. S. Jur, "Fabric-based wearable dry electrodes for body surface biopotential recording," *IEEE Trans. Biomed. Eng.*, vol. 63, no. 2, pp. 423–430, Feb. 2016.

Murat A. Yokus received the B.S. degree in textile engineering from Uludag University, Bursa, Turkey, and the M.S. degree from North Carolina State University, Raleigh, NC, USA. He is currently pursuing the Ph.D. degree in electrical engineering, and fiber and polymer science with the Department of Electrical and Computer Engineering and the Department of Textile Engineering, Chemistry, and Science, North Carolina State University, Raleigh, NC. He is currently a Board Member with the NC Fulbright Association Chapter. He was a recipient of the Fulbright Scholarship from the Bureau of Educational and Cultural Affairs of the U.S. Department of State from 2011 to 2013.

Rachel Foote is an undergraduate student at North Carolina State University, majoring in textile engineering, chemistry and science.

Jesse S. Jur received the B.S. degree in chemical engineering from the University of South Carolina, Columbia, SC, USA, in 2001, the M.S. degree in chemical and biomedical engineering from Johns Hopkins University, Baltimore, MD, USA, in 2004, and the Ph.D. degree in materials science and engineering from North Carolina State University, Raleigh, NC, USA, in 2007.

From 2009 to 2010, he was a Research Assistant Professor of Chemical and Biomolecular Engineering at North Carolina State University. He is currently an Assistant Professor of Textile Engineering, Chemistry, and Science with North Carolina State University. His current research interests are focused on integrating new nanotechnology methods for supporting electronic materials and devices in wearable fabrics.